INFECTION AND IMMUNITY, Sept. 2008, p. 3854–3868 Vol. 76, No. 9
0019-9567/08/$08.00+0 doi:10.1128/IAI.00072-08

EspF Interacts with Nucleation-Promoting Factors To Recruit Junctional Proteins into Pedestals for Pedestal Maturation and Disruption of Paracellular Permeability▽

Janneth Peralta-Ramírez,[1] J. Manuel Hernandez,[1] Rebeca Manning-Cela,[2] José Luna-Muñoz,[3] Carlos Garcia-Tovar,[4] Jean-Philippe Nougayréde,[5] Eric Oswald,[5] and Fernando Navarro-Garcia[1]*

Departments of Cell Biology,[1] Molecular Biomedicine,[2] and Physiology, Biophysics and Neurosciences,[3] Centro de Investigación y de Estudios Avanzados (CINVESTAV-IPN), Ap. Postal 14-740, 07000 Mexico DF, Mexico; Morphology Unit, Universidad Nacional Autónoma de México (UNAM-FES Cuautitlan), Ap. Postal 54714, Cuautitlan, Mexico[4]; and Unité des Microbiologie Moléculaire (INRA-ENVT), Ecole Nationale Vétérinaire, 31000 Toulouse Cedex 3, France[5]

Received 18 January 2008/Returned for modification 17 March 2008/Accepted 9 June 2008

Many pathogenic bacteria subvert normal host cell processes by delivering effector proteins which mimic eukaryotic functions directly into target cells. EspF is a multifunctional protein injected into host cells by attaching and effacing pathogens, but its mechanism of action is not understood completely. In silico analyses of EspF revealed two key motifs: proline-rich domains and PDZ domain binding motifs. Such functional domains may allow EspF to act as an actin nucleation-promoting factor by mimicking host proteins. In agreement with these predictions, we found that EspF from rabbit enteropathogenic *Escherichia coli* (E22) participates in the regulation of actin polymerization by binding to a complex of proteins at the tight junctions (TJ). EspF bound to actin and profilin throughout the course of infection. However, after 2 h of infection, EspF also bound to the neural Wiskott-Aldrich syndrome protein and to the Arp2/3, zonula occludens-1 (ZO-1), and ZO-2 proteins. Moreover, EspF caused occludin, claudin, ZO-1, and ZO-2 redistribution and loss of transepithelial electrical resistance, suggesting that actin sequestration by EspF may cause local actin depolymerization leading to EspF-induced TJ disruption. Furthermore, EspF caused recruitment of these TJ proteins into the pedestals. An E22 strain lacking EspF did not cause TJ disruption and pedestals were smaller than those induced by the wild-type strain. Additionally, the pedestals were located mainly in the TJ. The overexpression of EspF caused bigger pedestals located along the length of the cells. Thus, actin sequestration by EspF allows the recruitment of junctional proteins into the pedestals, leading to the maturation of actin pedestals and the disruption of paracellular permeability.

Many pathogenic bacteria subvert normal host cell processes through a complex cross talk with their mammalian hosts by delivering a collection of virulence factors named effector proteins directly into target cells (8). A common and recurring target of such effector molecules is the host cytoskeleton (13). Although structurally divergent due to their different tasks, these sophisticated effectors often mimic the functions of eukaryotic proteins (43). Both intracellular and extracellular bacteria that produce such targeted effector proteins often possess the ability to produce unique actin-rich structures within distinct regions of the host cells. In contrast to intracellular bacteria, which subvert cellular actin dynamics to facilitate their movement within the host cytosol and infection of neighboring cells, the attaching and effacing (A/E) pathogens do not enter the host cell but attach intimately to the cell surface, inducing motile actin-rich pedestals (13, 39).

A/E pathogens comprise enteropathogenic *Escherichia coli* (EPEC), enterohemorrhagic *E. coli* (EHEC), *Citrobacter rodentium*, and *Hafnia alvei* as well as animal EPEC strains such as rabbit EPEC (REPEC). EPEC, a diarrheagenic pathogen of importance in developing countries, is a gram-negative bacterium that stimulates the formation of A/E lesions in order to promote colonization of the intestine, resulting in damage to epithelial surfaces and diarrhea (17). A/E lesions are characterized by a localized loss of microvilli and intimate adherence of bacteria to the mammalian cell plasma membrane, followed by recruitment of F-actin to sites of bacterial attachment and ultimately resulting in the formation of actin-rich structures called pedestals (29). The genes necessary for A/E lesion formation in EPEC map to a 35-kb chromosomal pathogenicity island designated the locus of enterocyte effacement (LEE) (26). The LEE encodes components of the type III secretion system (T3SS), transcriptional regulators, chaperones, and T3SS effector proteins; the latter are translocated directly into host cells. One effector that is essential for actin assembly by A/E pathogens is the translocated intimin receptor, Tir (19). Upon entry into the cells, Tir is inserted into the plasma membrane in a hairpin-loop conformation exposing a central extracellular domain that binds to intimin, a bacterial adhesin of these A/E pathogens. Intimin clusters Tir in the plasma membrane and initiates pedestal formation (7).

Tyrosine-474, which is present in the cytoplasmically located

* Corresponding author. Mailing address: Department of Cell Biology, Cinvestav-Zacatenco, Ap. Postal 14-740, 07000 Mexico DF, Mexico. Phone: (525) 5061-3990. Fax: (525) 5061-3393. E-mail: fnavarro@cell.cinvestav.mx.

▽ Published ahead of print on 16 June 2008.

TABLE 1. Bacterial strains used in this study

Strain	General description	Reference
E22	Wild-type REPEC O103:K-:H2; rhamnose-negative strain	24
E22-red	E22 transformed with pDsRed1-1 (Amp^r)	This work
E22 Δ*espF*	E22 *espF*::*frt*; EspF mutant (Kan^r)	This work
E22(p*espF*-His)	E22 transformed with *espF* from E22 cloned into pET32b$^+$ His vector (Amp^r Kan^r)	This work
E22 Δ*espF*(p*espF*-His)	E22 Δ*espF* transformed with *espF* from E22 cloned into pET32b$^+$ His vector (Amp^r Kan^r)	This work
E22 Δ*escN*	E22 Δ*escN*; EscN mutant (Kan^r)	24

C-terminal domains of EPEC Tir, is phosphorylated by mammalian kinases (36), a modification required for efficient initiation of actin polymerization. A phosphorylated 12-residue peptide encompassing Y474 directly recruits the mammalian adaptor proteins Nck1 and Nck2 (5), which are known activators of the neural Wiskott-Aldrich syndrome protein (N-WASP)–Arp2/3 pathway of actin assembly in host cells (38). This actin nucleation activity can be triggered by the binding of N-WASP, a member of the WASP/Scar family of cellular actin nucleation-promoting factors (31). N-WASP has a highly modular domain structure: the C-terminal WA domain binds directly to and activates the Arp2/3 complex, while the N-proximal WASP homology 1 (WH1) domain binds the proline-rich F-actin- and Nck-binding WASP-interacting protein (WIP) (25, 30). N-WASP and Arp2/3 localize to both EPEC and EHEC pedestals (12, 16), and N-WASP is essential for the local recruitment of Arp2/3 and for pedestal formation by EPEC (16). The ability of N-WASP to stimulate the Arp2/3 complex can be activated by Rho family GTPases, but inhibitors of these GTPases do not inhibit pedestal formation by EPEC (4). However, the adapter protein Nck, which binds to phosphotyrosine residues via a Src homology 2 (SH2) domain, can functionally substitute for Cdc42 in stimulating N-WASP to trigger actin polymerization in vitro (38). Furthermore, tyrosine-454, which is also C-terminally located within EPEC Tir, is also phosphorylated, although inefficiently. This residue contributes to an Nck-independent signaling cascade leading to actin assembly at relatively low levels (6).

In addition to delivering Tir, EPEC delivers other effector proteins, such as EspF, into the host cell via the T3SS (26). In vitro studies have demonstrated that the EPEC effector protein EspF plays a central role in decreasing transepithelial electrical resistance (TER) and altering the intestinal epithelial tight junction (TJ) structure (28, 42, 48). Specifically, EPEC disrupts the TJ architecture, as evidenced by a loss of TJ protein-protein interactions, the redistribution of TJ proteins, and the appearance of aberrant TJ strands in the lateral membrane (32). Although the mechanism by which EspF perturbs the intestinal barrier function in vitro has not been defined, it is known that strains deficient in *espF* are not attenuated in their abilities to form characteristic A/E lesions (27, 28). In addition to these morphological and physiological changes, EPEC also causes the dephosphorylation of occludin (42). Zonula occludens-1 (ZO-1) distribution has also been shown to be altered following EPEC infection (37). However, the effects on TJ strands and individual TJ protein-protein interactions have not been examined.

Thus, EspF has clearly been associated with TJ disruption but not with pedestal formation (27). However, here we showed that EspF contains proline-rich sequences and PDZ domain binding motifs, domains which are relevant for protein interactions with actin regulator proteins as well as TJ proteins, suggesting a key role for EspF in pedestal maturation and the disruption of paracellular permeability.

MATERIALS AND METHODS

Bacterial strains, plasmids, and culture conditions. Strains used in this study are listed in Table 1. Bacterial cultures were grown overnight in Luria-Bertani (LB) broth in a shaking incubator (150 rpm). Depending on the plasmid (Table 1), ampicillin and/or kanamycin was added to the LB media (100 μg/ml and/or 35 μg/ml, respectively). The *E. coli* E22 wild-type strain was transformed with plasmid pDsRed1-1 to obtain the red fluorescent bacteria or with p*espF*-His to obtain an EspF-overexpressing strain. Other strains were transformed with a plasmid that encodes EspF recombinant protein (p*espF*-His). Unless otherwise mentioned, all the reagents used were obtained from Sigma-Aldrich, Inc.

p*espF*-His construction. The *espF* gene was amplified from genomic DNA of *E. coli* E22 by use of Herculase polymerase (New England Biolabs, Inc.) and the following primers: forward 5′, GGC CCA AGC TTG ATG CTT AAT GGA ATT AGT CAA G; and reverse 5′, CGT CGA CGC GTC TGC AGT TTC TGC CTT TTT CGA CAG TTC ATA G. The PCR product (645 bp) was purified by use of a QIAquick PCR kit (Qiagen, Inc.) and cloned into pGEM-T Easy vector (Promega Corp.) according to the manufacturer's instructions to create pGEM-T-EspF. Subsequently, the *espF* gene was subcloned into the pET32b vector by digestion with HindIII/SalI (New England Biolabs, Inc.) to obtain the polyhistidine-tagged EspF fusion protein EspF-His. DH10B bacteria were transformed with p*espF*-His to obtain the recombinant histidine-tagged EspF.

***espF* mutant construction.** To generate an *espF* deletion mutant of strain E22, the *espF* gene was replaced by a gene encoding kanamycin resistance by use of the lambda red recombinase system (9). The kanamycin resistance gene was amplified from pKD4 by PCR with primers espF-FRT-sense (5′-AAT TAG TCA AGC TGT TTC TAC ACT AGG ACG GCA TAT TAC TAG TGC GGC AAT GTA GGC TGG AGC TGC TTC G) and espF-FRT-antisense (5′-CCG GGC GGC TTG GCT TAA GAC CTG AAG TAT CAA GAC TTT TCG ATT TTT CAC ATA TGA ATA TCC TCC TTA G). The product was treated with DpnI and introduced into E22 carrying pKD46. Colonies containing the *espF*::Kan knockout were then obtained as described previously (9).

Cell culture. RK13 rabbit kidney cells (CCL-37; ATCC) were propagated in humidified 5% CO_2-95% air at 37°C in Dulbecco's modified Eagle's medium (DMEM; Invitrogen Ltd.) supplemented with 10% fetal bovine serum (HyClone Ltd.), 0.1 mM nonessential amino acids, 2 mM L-glutamine, penicillin (1,000 units/ml), and streptomycin (100 μg/ml). The cells were serially propagated after harvesting with 10 mM EDTA and 0.25% trypsin (Invitrogen Ltd.) in phosphate-buffered saline (PBS; pH 7.4) solution. For experimental use, subconfluent RK13 cells were resuspended with EDTA-trypsin, plated into eight-well LabTek slides (VWR Ltd.), and allowed to grow to 95% confluence.

Transfection of RK13 cells. RK13 cells were transfected with the plasmid pActin-EGFP or with pEGFP as a control (BD Biosciences Clontech Ltd.) by use of the calcium phosphate method. Transfection was performed with 10 μg of cesium chloride-purified plasmids. The transfection efficiency was 20 or 15%, respectively. Stable transformed RK13 cell lines (RK13 expressing actin-green fluorescent protein [GFP] [RK13-actin-GFP] or RK13-GFP) were selected by adding (48 h posttransfection) 350 μg/ml of Geneticin G-418 (Invitrogen Ltd.) and then maintained in DMEM. RK13-actin-GFP cells were cloned by limiting dilution on 96-well tissue plates and the clones selected by epifluorescence were analyzed and sorted by fluorescence-activated cell sorting in order to obtain clones expressing fluorescent actin. Cells containing exogenous fluorescent actin

maintained the sensitivity to actin-altering drugs and did not show any alteration in the actin cytoskeleton.

Infection assay. Overnight bacterial cultures, grown in LB, were diluted (1:15) with serum- and antibiotic-free DMEM and incubated at 37°C until the mid-log phase of growth was achieved. RK13 cells (6×10^5) expressing actin-GFP or GFP were seeded on eight-well chamber slides (Nunc, Lab-Tek). When the cells reached a confluence of 95%, the monolayer was washed with PBS and then infected with bacteria to a multiplicity of infection of 100 in DMEM and maintained for 1 h in a humid incubator at 37°C with an atmosphere of 5% CO_2. Afterwards, the medium was aspirated, and the nonadherent bacteria were removed by gentle washing with PBS. The monolayer was covered with fresh medium and the remaining adherent bacteria were allowed to infect the cell for 6 h (or the indicated times).

Measurement of TER. TER of cultured monolayers was determined directly using an EVOM epithelial voltohmmeter. Briefly, 1×10^5 RK13 cells or 6×10^4 MDCK cells were seeded in 6.5-mm permeable transwell supports (3.0 μm pore size; Corning, Inc.). The electrodes were cleaned with 70% ethanol and rinsed with sterile PBS before measurements were taken. One electrode was immersed in the medium over the monolayers, while the other one was immersed in the medium outside the transwell. The resistance was registered in $\Omega \cdot cm^2$. When the resistance was stable, the monolayers were washed with PBS and infected as described above with the strains listed in Table 1, and TER was quantified every hour for periods lasting 6 h for RK13 and 12 h for MDCK experiments. The resistance data obtained from three independently analyzed monolayers were adjusted to those obtained for the control and are reported as relative percentages.

Immunoprecipitation assays. Confluent monolayers of RK13 cells were infected with *E. coli* E22 (multiplicity of infection of 100) for 1, 1.5, 2.0, 2.5, and 3.0 h. Uninfected and infected monolayers were washed with cold PBS, and then the cells were removed with a scraper and lysed by incubation with radioimmunoprecipitation assay (RIPA) buffer (50 mM Tris-HCl, 150 mM NaCl, 1% NP-40, 0.5% sodium deoxycholate, 1 mM Na-vanadate, 1 mM phenylmethylsulfonyl fluoride, and protease inhibitor mix) for 30 min at 4°C. The cell extracts were centrifuged at $13,000 \times g$ for 15 min at 4°C and the supernatant fraction, containing soluble "cytoplasmic" components, was removed and kept on ice. Subsequently, the cell pellet was rinsed in PBS, resuspended in a buffer {5 mM HEPES, 5 mM 3-[(3-cholamidopropyl)-dimethylammonio]-1-propanesulfonate (CHAPS), 5 mM dithiothreitol, and 150 mM NaCl, pH 7.5}, and centrifuged again ($13,000 \times g$, 15 min at 4°C), and the CHAPS-soluble "membrane" fraction was removed and kept on ice. The protein concentrations of all samples were determined by the Bradford method and equal amounts of protein were used for the immunoprecipitation assays. For EspF immunoprecipitation experiments, 5 μg of anti-EspF monoclonal antibody (a gift from Michael Donnenberg, Department of Microbiology and Immunology, University of Maryland, Baltimore, MD) and protein A beads (Sigma) were incubated with cell lysates for 3 h at 4°C to precipitate the protein-antibody complex. The beads were washed three times with RIPA buffer. The protein was eluted with Laemmli sample buffer (21) and boiled for 10 min before Western blot analysis.

Western blotting. Protein samples from immunocomplexes were loaded and resolved by sodium dodecyl sulfate-polyacrylamide gel electrophoresis (SDS-PAGE). Electrophoresed proteins were transferred to nitrocellulose membranes (45) and then blocked with 5% skim milk. Membranes were then probed with antibodies directed against occludin (mouse monoclonal antibody, 1:200), claudin (rabbit polyclonal antibody, 1:200), ZO-1 (rabbit polyclonal antibody, 1:200), ZO-2 (rabbit polyclonal antibody, 1:200; Zymed Laboratories, Inc.), profilin (goat polyclonal antibody, 1:100); Arp-2 (goat polyclonal antibody, 1:100), WASP (rabbit polyclonal antibody, 1:100; Santa Cruz Biotechnology, Inc.), EspF (mouse monoclonal antibody, 1: 200; described above), and actin (mouse monoclonal, 1:200; prepared in our laboratory). Primary antibodies were probed with peroxidase-conjugated secondary antibodies (Zymed Laboratories) and detected using the ECL chemiluminescence substrates according to the manufacturer's instructions (GE Healthcare).

Measurement of pedestal number and size. Pedestals were visualized as elongated structures characterized by actin-GFP-enriched structures as previously reported for EPEC infections by use of the fluorescence actin staining test (20). For pedestal quantification, a temporal course of REPEC infection was performed at 30-min intervals up to 4 h postinfection. Fixed cells were analyzed under a confocal microscope by taking five photographs of randomly selected fields for each time point. Each experiment represented 50 cells and was repeated at least three times. Each photograph was analyzed by the Image-Pro Plus software (version 6.0) using the manual count mode and spatial calibration (μm units calibrated by using the confocal microscopy scale) to establish the number and size of the pedestals, respectively. Pedestal number data were plotted as the average number of pedestals per cell. Pedestal size data were plotted as the average size of pedestals during the temporal course of infections.

Immunofluorescence and confocal microscopy. At different times postinfection, uninfected and REPEC-infected RK13 cells expressing actin-GFP were processed at room temperature for immunofluorescence to analyze infection progress, pedestal formation, and the presence of TJ proteins. Cell monolayers were fixed with 3.7% formaldehyde, permeabilized with 0.5% Triton X-100 for 10 min, and blocked with 0.1% bovine serum albumin for 20 min (all solutions were diluted with PBS). The fixed monolayers were stained using commercially available antibodies (mouse anti-occludin [1:20], rabbit anti-claudin [1:20], rabbit anti-ZO-1 [1:20], and rabbit anti ZO-2 [1:20] [Zymed Laboratories]), followed by incubation with Cy5- or rhodamine-conjugated goat anti-rabbit or goat anti-mouse secondary antibodies (1:50) for 1 h. The samples were mounted on slides in Gelvatol 20/30 (Monsanto, Inc.) and analyzed on a Leica TCS-P2 confocal laser scanning inverted microscope using the 100× oil immersion plan apochromatic objective (numerical aperture, 1.4). Six to 10 consecutive single sections were obtained per sample in the *z*-axis plane. To avoid the fluorescence filter, each channel was captured independently. GFP was excited at 488 nm, DsRed1-1 protein or rhodamine at 560 nm, and Cy5 at 650 nm. The images obtained were grouped, projected, and analyzed with Leica Lite software and/or Image-Pro Plus version 6.0 software.

RESULTS

EspF has affinity for profilin, Arp2/3, and actin. Since EspF is a multifunctional protein and many T3SS effectors mimic actin-associated proteins, we investigated by using position-specific iterated BLAST (PSI-BLAST), which is useful for finding very distantly related proteins, whether the *E. coli* E22 allele of EspF had homology with any eukaryotic actin-associated proteins. EspF had 28% identity to human WASP, 28% to human and mouse WAVE-Scar, 30% to human and mouse WIP, 31% to RickA (a WASP-like protein from *Rickettsia* sp.), and 32% to human and mouse N-WASP and mouse Enah (protein defined structurally by a proline-rich core domain, which is important for interaction with the small actin-binding protein profilin). In fact, the homology between EspF and these WASP-related proteins was based on their proline-rich repeats. EspF analysis by eukaryotic linear motif software showed that EspF from REPEC E22 has three identical proline-rich sequences (RPAPPPP), each separated from the next by 41 amino acids, which can be recognized by class I SH3 domains, such as those of proteins interacting with the WASP-related proteins. Additionally, REPEC EspF has three identical class III PDZ domain binding motifs (KDHL) between each proline-rich repeat, each separated from the next by 43 amino acids (Fig. 1). Furthermore, EspF from EPEC strain E2348/69 has exactly the same motifs in the same positions plus two other class III PDZ domain binding motifs (SETV), each one located precisely between a KDHL motif and a proline-rich repeat (Fig. 1). Interestingly, EspF from EHEC has exactly the same motifs in the same positions as those present in EPEC EspF (with slight sequence variations) but containing another set of PDZ domain binding motifs (PEAL and KDHL), with a proline-rich repeat between them. EspF from *C. rodentium* is much like REPEC EspF but contains two other sets of proline-rich repeats and KDHL motifs (Fig. 1).

Using the aligned amino acid sequences of the WASP-related proteins, RickA proteins, and *E. coli* EspF, we generated a phylogenetic tree (CLC Free Workbench 4.0). In contrast to the bacterial RickA protein, which clustered with the WASP and N-WASP proteins (Fig. 2A), *E. coli* EspF clustered with the WIP proteins (Fig. 2A), suggesting that EspF may be functionally related to the WIP proteins. Furthermore, align-

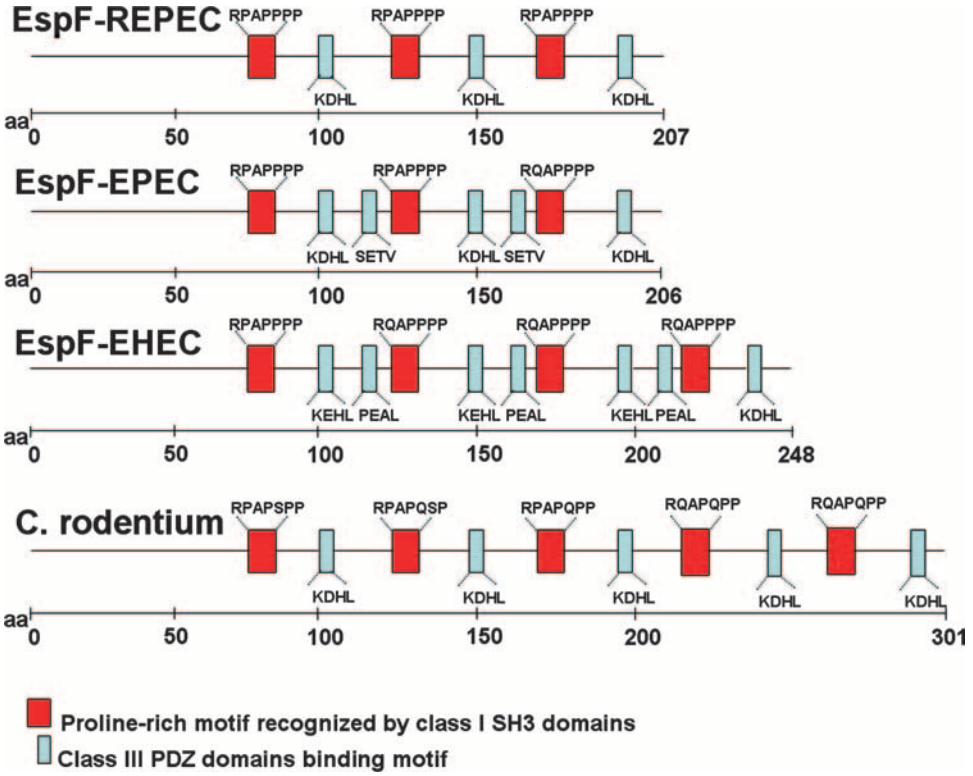

FIG. 1. Schematic representation of repeat motifs into EspF orthologs. EspF sequences from REPEC (E22) AAF03351, EPEC (2348/69) AAC38400, EHEC (O157:H7, Sakai) BAB37973, and *Citrobacter rodentium* AAL06387 were analyzed by eukaryotic linear motif software and the common motifs were drawn as boxes in the indicated positions into the amino acid sequences.

ment of *E. coli* EspF, N-WASP, and WIP showed that these proteins share conserved motifs important for binding to profilin, Arp2/3, and actin (Fig. 2B). Together, these data suggest that proline-rich repeats may be essential for the function of EspF and that the repeats may play a role in pedestal formation through recruitment of host cytoskeletal proteins.

Since EspF may possess WIP-like features, we tested by immunoprecipitation whether EspF had affinity for WIP-inter-

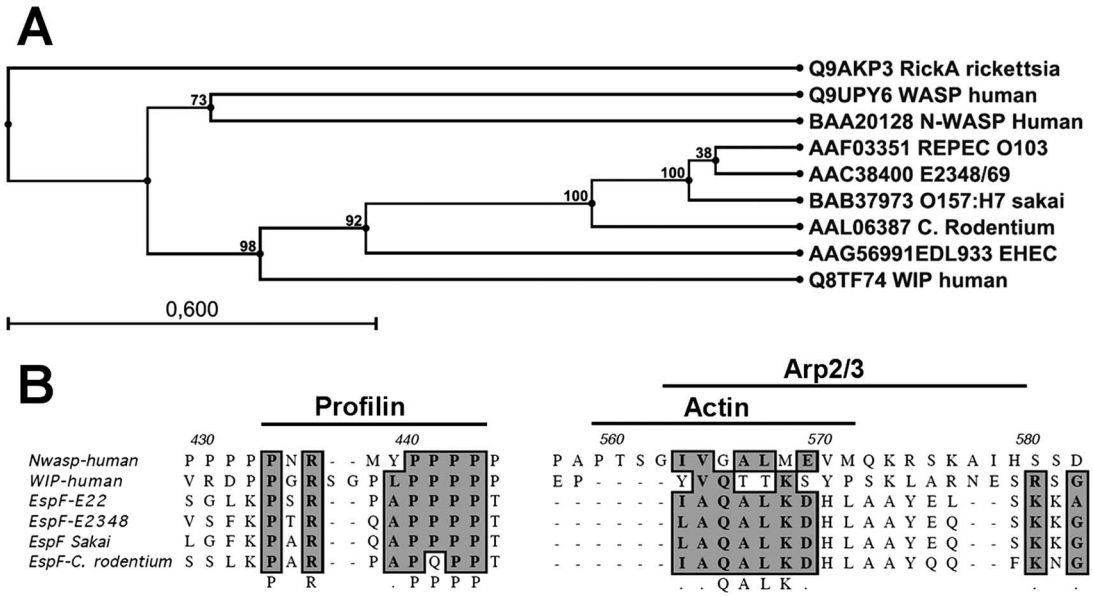

FIG. 2. Alignment of the EspF orthologs with human N-WASP and WIP. (A) Phylogram of EspF sequences and of WASP, N-WASP, WIP, and RickA genes currently available in public databases. (B) Amino acid sequence alignment of EspF orthologs, WIP, and N-WASP. Two relevant portions are shown and the positions of the potential profilin-, G-actin-, and Arp2/3-binding motifs are indicated over the amino acid sequences.

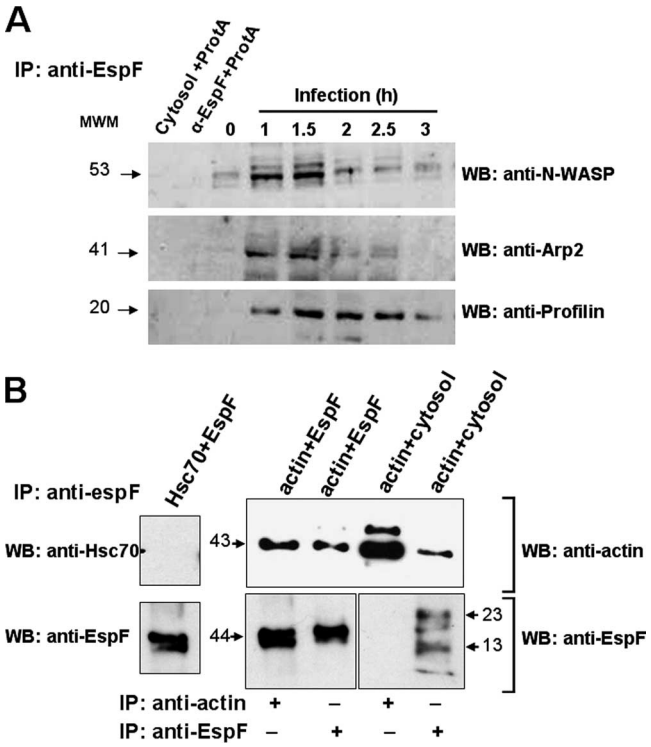

FIG. 3. EspF binds N-WASP, Arp2/3, profilin, and actin. (A) Coimmunoprecipitation of N-WASP, Arp2/3, and profilin by anti-EspF antibody. RK13 cells were infected with wild-type E22 at various times. After infection, cells were fractionated and the soluble fraction was immunoprecipitated with an anti-EspF antibody. Immunocomplexes were separated by SDS-PAGE, transferred to nitrocellulose membrane, and probed with antibodies against N-WASP, Arp2, and profilin by Western blotting (WB). Soluble fractions plus protein A-agarose (Cytosol+ProtA) and anti-EspF antibody plus protein-A-agarose (α-EspF+ProtA), as well as infection at time zero, were used as negative controls. MWM, molecular weight marker. (B) Coimmunoprecipitation of actin and EspF. Five-microgram portions of purified actin and recombinant EspF-His were mixed. The mix was subjected to immunoprecipitation by using anti-EspF or anti-actin antibodies. As a negative control, purified EspF was mixed with commercial Hsc70 and the immunoprecipitation was performed with anti-EspF antibodies. Additionally, soluble fractions from infected cells were mixed with 5 μg of actin, subjected to immunoprecipitation, and then analyzed by Western blotting as indicated above. IP, immunoprecipitation.

acting proteins such as profilin, Arp2/3, WASP, and actin. RK13 cells were infected with REPEC E22 at various times. At different time points after infection, cells were lysed and subjected to immunoprecipitation with anti-EspF antibodies. The immunoprecipitates were analyzed by Western blotting using anti-profilin, anti-Arp2, anti-WASP, and anti-actin antibodies. Arp2/3 and WASP clearly coimmunoprecipitated with EspF at 1 and 1.5 h postinfection and did so slightly at 2 and 2.5 h, but no interaction was observed at 3 h postinfection (Fig. 3A). Interestingly, profilin coimmunoprecipitated with EspF at all time points tested (1 to 3 h postinfection) (Fig. 3A). Similarly, actin also coimmunoprecipitated with EspF at all time points (see Fig. 12A). Surprisingly, the anti-EspF coimmunoprecipitated a significant amount of actin, suggesting that EspF may interact directly with actin but also indirectly through profilin (since both proteins coimmunoprecipitated with EspF through the course of infection). To test this hypothesis, purified actin and EspF were mixed together and subsequently subjected to immunoprecipitation with either anti-EspF or anti-actin before analysis by Western blotting using either anti-EspF or anti-actin. As a negative control, purified EspF was mixed with commercial Hsc70, a protein unable to interact with EspF (34). Additionally, purified actin was added to soluble fractions from lysed REPEC-infected cells and was also subjected to the same analysis. Both anti-actin and anti-EspF were able to coimmunoprecipitate EspF and actin, respectively (Fig. 3B), indicating that EspF is able to bind actin directly. Interestingly, the anti-EspF antibody coimmunoprecipitated actin from the cytosolic fraction of REPEC-infected cells supplemented with an excess of purified actin, indicating that endogenous EspF (present in the cytosolic fraction) was also able to bind exogenous purified actin, since the band of immunoprecipitated actin was similar to that observed in the in vitro experiment, where a mixture of 5 μg of EspF-actin purified proteins was used. In contrast, immunoprecipitation of EspF by the anti-actin antibody was significantly reduced by the presence of an excess amount of actin (Fig. 3B). All of these data suggest that EspF binds directly to actin and also indirectly to actin by binding profilin.

REPEC induces A/E lesions in actin-GFP-transfected RK13 cells. An experimental cellular model was used to investigate the role of EspF as a mimic of actin-associated proteins during an EPEC infection. RK13 cells from rabbit kidneys were transfected with the plasmid p-actin-GFP, and these transfected cells were subsequently used in infection assays with *E. coli* E22 cells that had been transformed with the plasmid pDsRed1-1 to obtain red fluorescent bacteria (E22-RFP). Actin-GFP-transfected RK13 cells (Fig. 4C) were stained with phalloidin-rhodamine (Fig. 4B) to determine the formation of exogenous actin filaments, which were detected in yellow in merged images from transfected cells (Fig. 4A), while untransfected cells showed red actin filaments. Transfected RK13 cell clones were selected with 350 μg/ml of Geneticin G418 to obtain stable clones expressing actin-GFP. These actin-GFP-transfected cells (green) were infected with E22-RFP (red) for 6 h and then fixed and directly observed by confocal microscopy. Under these conditions, the pedestals (green) were easily observed (Fig. 4D) beneath attached bacteria (red) throughout the cytoplasm (Fig. 4F). Therefore, this model can be used to study the dynamics of pedestal formation and the bacterial effector proteins that mimic the functions of host cell proteins during actin polymerization.

REPEC EspF redistributes TJ proteins and increases the pedestal length. An interesting hypothesis arising from the previous results is that actin and profilin sequestration by EspF may influence the actin polymerization-depolymerization activity at the TJs, thereby leading to the redistribution of TJ proteins (46). To test this hypothesis, RK13 cells expressing actin-GFP were infected for 4 h with wild-type E22, an isogenic EspF mutant (E22 Δ*espF*), the isogenic mutant complemented with p*espF* [E22 Δ*espF*(p*espF*)], or the wild-type E22 transformed with p*espF* [E22(p*espF*)]. Redistribution of TJ proteins was immunodetected by using anti-ZO-1 and anti-ZO-2 antibodies. We used a T3SS mutant (E22 Δ*escN*) as a negative control, as it was previously demonstrated that it could not cause pedestal formation and redistribution of junctional proteins such as ZO-1 and ZO-2 (Fig. 5A and B). As previously

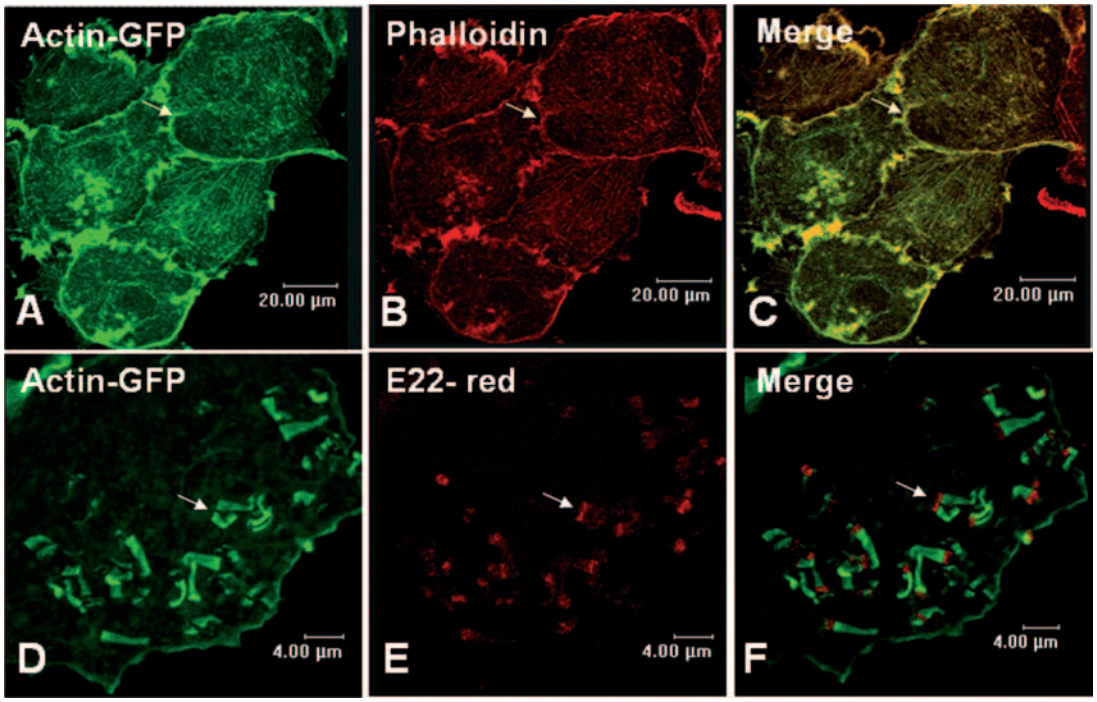

FIG. 4. Red fluorescent REPEC (E22) induces actin filament rearrangement and A/E lesions in RK13 cells expressing actin-GFP. (A to C) Colocalization of stable actin-GFP expressed in RK13 cells and F-actin decorated with phalloidin. Uninfected RK13 cells expressing stable actin-GFP (A) were fixed and stained with rhodamine-phalloidin (B), and the resultant images were merged (C). Colocalization was integrated in stress fibers and lamellipodium structures (arrows). (D to F) Cytoskeleton rearrangements and formation of actin-rich pedestals beneath the attached bacteria in RK13 cells expressing actin-GFP. RK13 cells expressing stable actin-GFP (D) were infected for 6 h with red fluorescent E22 (E), and the resultant images were merged (F). Arrows show actin-rich pedestals beneath the attached bacteria.

shown (24), wild-type E22 was able to cause pedestal formation, and it was also able to cause redistribution of the ZO-1 and ZO-2 junctional proteins (Fig. 5C and D). Thus, these data suggest that these events may be related, as redistribution of TJ proteins has been observed for all the wild-type A/E pathogens. EspF has been associated with TJ protein redistribution but not associated with pedestal formation (28). However, by using E22 Δ*espF*, we were able to find pedestals smaller than those seen for the wild-type strain and no ZO-1 and ZO-2 redistribution, as evidenced by the absence of red marks in the cytoplasm and their presence in the intercellular junctions (Fig. 5E and F). Furthermore, these smaller pedestals were located mainly at the intercellular junctions. Complementation of E22 Δ*espF* with the plasmid p*espF* reestablished the effects observed for the wild-type strain, i.e., normally sized pedestals, cytoplasmic redistribution of ZO-1 and ZO-2, and pedestal formation throughout the cells (Fig. 5G and H). Additionally, perhaps due to increased production of EspF in the complemented strain, a clearer colocalization of pedestals and ZO-1 and ZO-2 was seen (Fig. 5G and H; yellow pedestals). This was recently reported by Hanajima-Ozawa et al. (15), who showed recruitment of ZO-1 into pedestals caused by a human EPEC strain. Moreover, cells infected with the wild type transformed with p*espF* showed pedestals bigger than those seen in cells infected with the untransformed wild type (Fig. 5I and J).

To understand this relationship, we determined the pedestal length and number for and recorded the electrical resistance of an RK13 monolayer infected with these REPEC variants. The length and number of pedestals were quantified by the relative size (μm) of fluorescent actin bundles and the number of pedestals per cell, respectively. Interestingly, the increase in pedestal size depended on the presence of EspF. Thus, in a time course experiment the pedestals were detected at 1 h postinfection with E22 Δ*espF*, wild-type E22, and E22 Δ*espF*-(p*espF*), with various sizes (0.7, 1.4, and 1.7 μm, respectively), whereas the pedestals induced by the strain overproducing EspF [E22(p*espF*)] were detected at 30 min postinfection with sizes of about 1.2 μm (Fig. 6A). All pedestals grew to reach a stationary phase at 2 h postinfection with various sizes [for E22 Δ*espF*, 1.2 μm; for E22, 2 μm; for E22 Δ*espF*(p*espF*), 2.7 μm; and for E22(p*espF*), 3.2 μm]. However, the numbers of pedestals induced in the infected cells were almost identical for all strains, except for the *espF* isogenic mutant, which had less pedestals per cell, but only at 3 and 3.5 h postinfection (Fig. 6B). Interestingly, an increase in pedestal size for each REPEC variant correlated with a decrease in TER induced by these REPEC variants on RK13 cell monolayers (Fig. 6C). As RK13 cell monolayers had not been used previously to record TER values (the TER values we found were about 300 $\Omega \cdot cm^2$), we also corroborated the effects of the REPEC variants on MDCK cells, a classical model that forms strong TJs (with TER values of about 1,000 $\Omega \cdot cm^2$). We found similar results for both cell types (Fig. 6D). It is well known that EHEC forms smaller pedestals than does EPEC; therefore, we transformed EHEC EDL933 with p*espF* and used these constructs to infect HEp-2 cells to compare pedestal sizes against those induced by

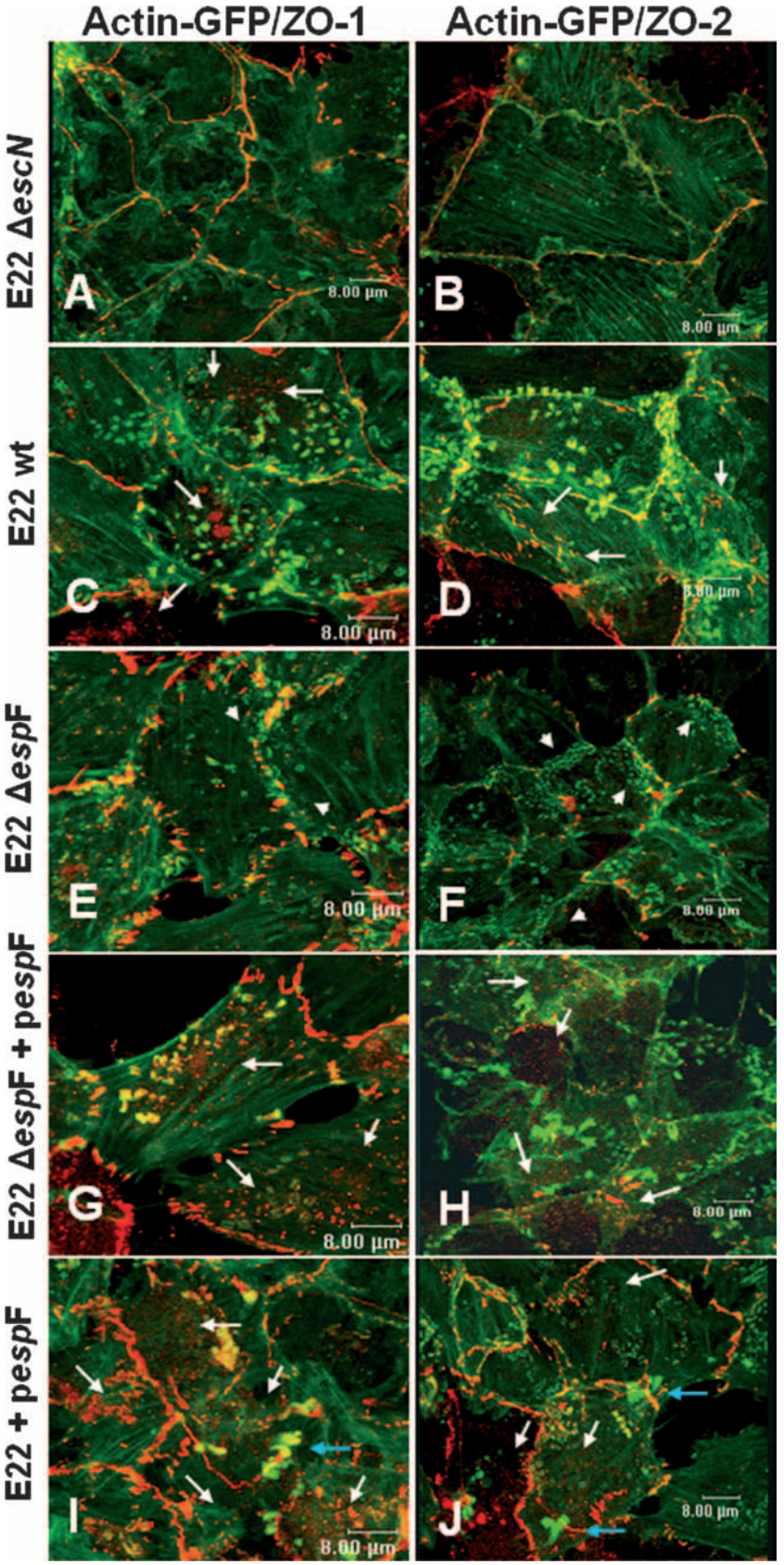

FIG. 5. EspF expression by E22 causes junctional protein recruitment to the pedestals and an increase in pedestal length. RK13 cells expressing actin-GFP were infected with a T3SS mutant (E22 Δ*escN* [control]; A and B), wild-type (wt) E22 (C and D), E22 Δ*espF* (E and F), E22 Δ*espF*

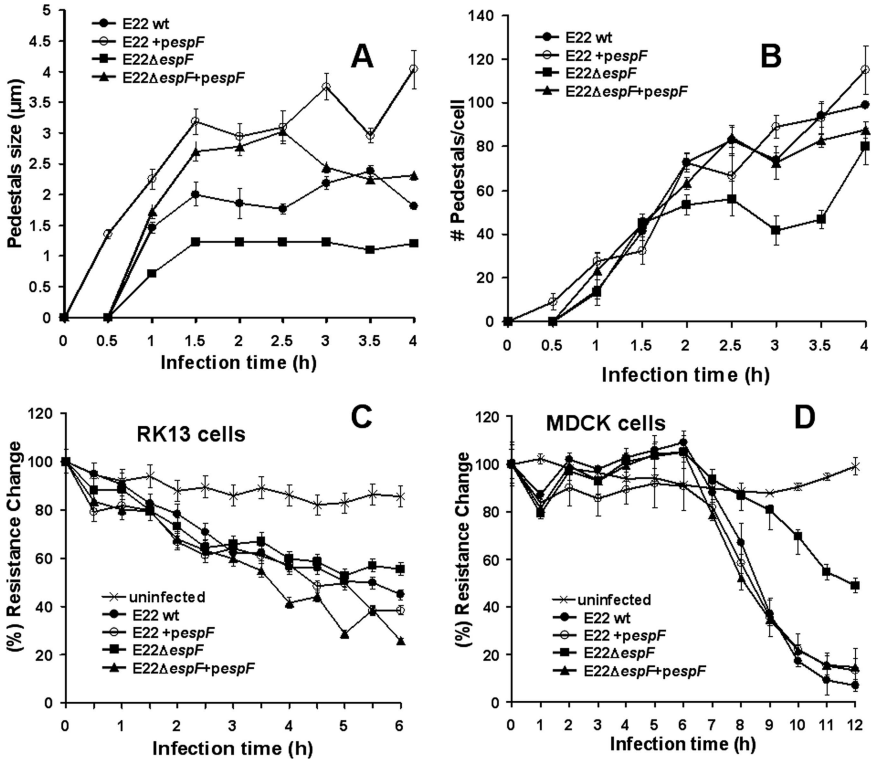

FIG. 6. Removing of junctional proteins by EspF-producing REPEC influences pedestal maturation and disrupts TJ barrier function. EspF increases the pedestal length. RK13-actin-GFP monolayers were infected with wild-type (wt) E22, E22 Δ*espF*, E22 Δ*espF*(p*espF*) (E22Δ*espF*+*espF*), or E22(p*espF*) (E22+p*espF*) for the times indicated in the graph. The temporal course of the infection was correlated with the sizes of pedestals (A) as well as with the number of pedestals per cell (B). Data were obtained using the Image-Pro Plus software, version 5.1, from three independent experiments for each infection. EspF decreases the TER. RK13 (C) and MDCK (D) monolayers were infected with the different strains indicated above for the times indicated in the graph, after which TER was recorded and expressed as resistance changes expressed as percentages. The data are averages of three measures from three independent experiments.

the EHEC wild type. EHEC(p*espF*) induced pedestals of 1.3 ± 0.4 μm, while those induced by the EHEC wild type were 0.6 ± 0.3 μm. The same results were found for similar experiments with RK13 cells (data not shown).

EPEC redistributes TJ proteins to recruit them into A/E lesions. Previous data indicated that EspF sequestered actin and profilin, leading to actin depolymerization and TJ redistribution, and suggest that TJ proteins may act as link proteins between the plasma membrane and actin-rich pedestals. To test this, we searched for redistribution of transmembrane junctional proteins (which may interact with ZO-1 and ZO-2) after REPEC infection. RK13 cells expressing actin-GFP were infected with red fluorescent *E. coli* E22, fixed, and immunostained with either anti-occludin or anti-claudin antibodies. Untreated cells showed both occludin and claudin proteins in the cell periphery (Fig. 7A to C and 8A to C, respectively). In contrast, infected cells showed redistribution of both transmembrane junctional proteins from TJs to the cytoplasm (Fig. 7D to F and 8D to F). Interestingly, occludin colocalized with the actin-rich pedestals, and the colocalization was detected along the pedestals and beneath the infecting bacteria (Fig. 7G to J), whereas claudin also colocalized with the pedestals but the colocalization was mainly at the tip of the pedestal and just under the infecting bacteria (Fig. 8G to J). These data indicate that EspF is able to cause the recruitment of transmembrane junctional proteins into the actin pedestals and suggest that these junctional proteins are important for maturation of the actin-rich pedestals, perhaps through connecting the membrane and the actin bundles.

Interaction of EspF with TJ proteins. To understand the relationship of EspF with actin pedestals or the TJ proteins in RK13 cells infected with the REPEC strain E22, we searched for EspF localization and its colocalization with ZO-1, ZO-2, claudin, and actin pedestals by immunofluorescence and confocal microscopy. RK13 cells expressing actin-GFP were infected with wild-type E22, E22 Δ*espF*, or E22(p*espF*) for 3 h.

complemented with p*espF* (E22Δ*esp*F+p*esp*F; G and H), and wild-type E22 transformed with p*espF* (E22+p*esp*F; I and J) for 4 h. Infected cells were stained with anti-ZO-1 (A, C, E, G, and I) or anti-ZO-2 (B, D, F, H, and J). The green and red channels were merged (white arrows point out ZO protein redistribution). Note that the *espF* mutant (E22 Δ*espF*) was unable to cause ZO-1 and ZO-2 rearrangements; therefore, the pedestals were formed in the intercellular junction (arrowheads). Also, the EspF-overexpressing strain [E22(p*espF*)] increased the recruitment of these junctional proteins to the pedestals as well as their length (blue arrows).

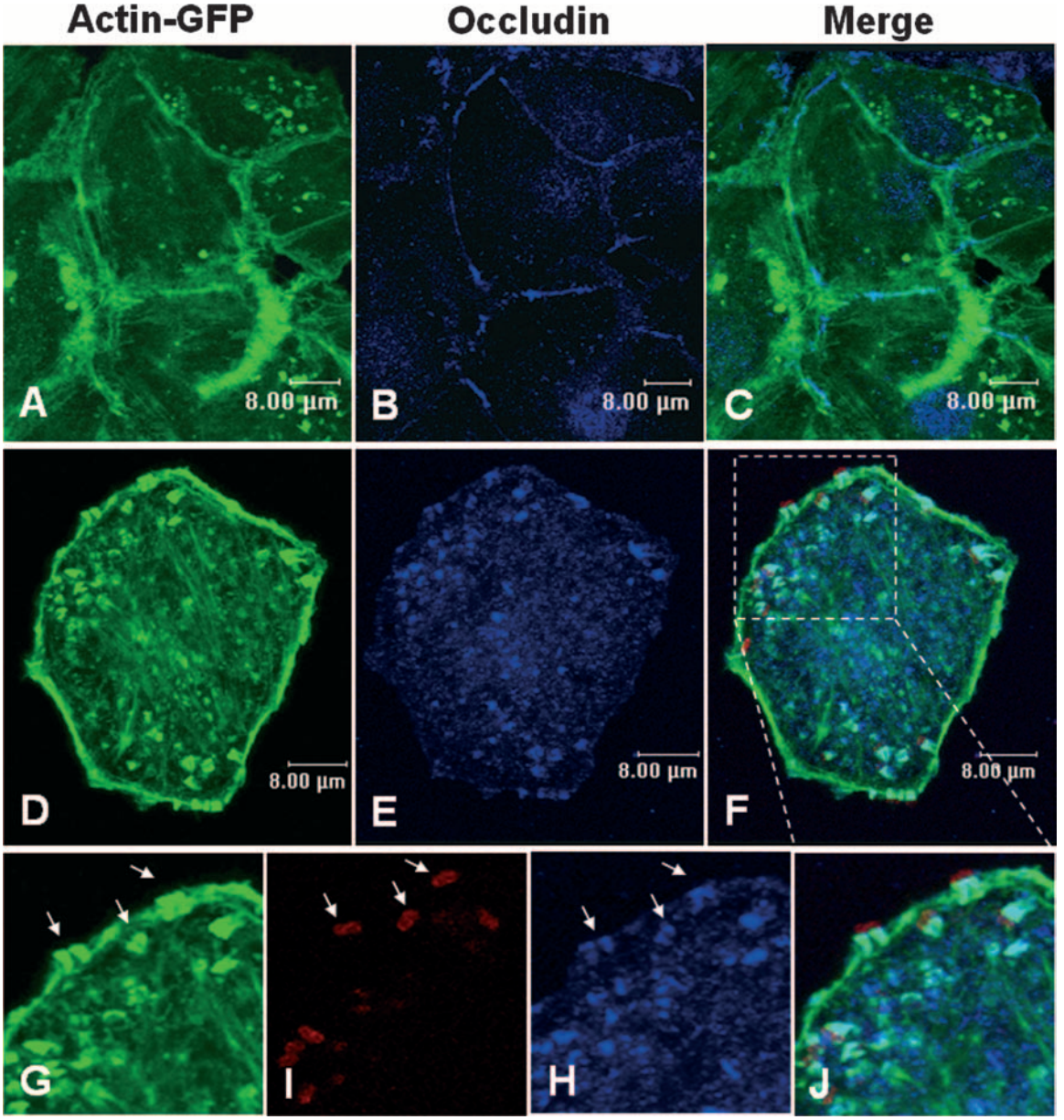

FIG. 7. REPEC induces occludin rearrangement and recruitment to pedestals in RK13 cells. (A to F) Rearrangement of occludin by REPEC (E22). Uninfected RK13 cells expressing actin-GFP (A) were fixed and stained with anti-occludin (B), and both images were merged (C). RK13 cells expressing actin-GFP (D) were infected with red fluorescent E22 (F) and then fixed and stained with anti-occludin (E), and the images were merged (F). (G to J) REPEC recruits occludin into the pedestals. The magnification of panel F shows the specific localization of actin-GFP pedestals (G) beneath the attached red bacteria (I), which are enriched with occludin (H). The merged images (C, F, and J) show the colocalization of actin-GFP pedestals and occludin.

Triple staining showed that EspF did not colocalize with ZO-1 (Fig. 9B to D), ZO-2 (Fig. 9F to H), claudin (Fig. 9J to L), or actin pedestals (Fig. 9A, E, and I), even though the three junctional proteins colocalized with the actin pedestals (Fig. 9D, H, and L). At 3 h postinfection, EspF was localized throughout the cytoplasm (Fig. 9B, F, and J). EspF was not detected in cells infected with E22 Δ*espF* (Fig. 10B, F, and J) but small pedestals were detected (Fig. 10A, E, and I). These small pedestals were localized mainly in the intercellular junctions, and they colocalized with the junctional proteins (Fig. 10D, H, and L), suggesting a key role for the junctional proteins in pedestal formation. In contrast, overexpression of EspF did not induce colocalization of EspF with the junctional proteins or the actin pedestals, but the three junctional proteins colocalized with the actin pedestals (Fig. 11D, H, and L) and many pedestals increased in length (Fig. 11A, E, and I). At 3 h postinfection, EspF was localized throughout the cytoplasm, apparently associated with vesicles or organelles (Fig. 11B, F, and J).

To further study the interaction of EspF with the junctional proteins and its relationship with actin, RK13 cells were infected with wild-type E22 at various times (every 30 min from

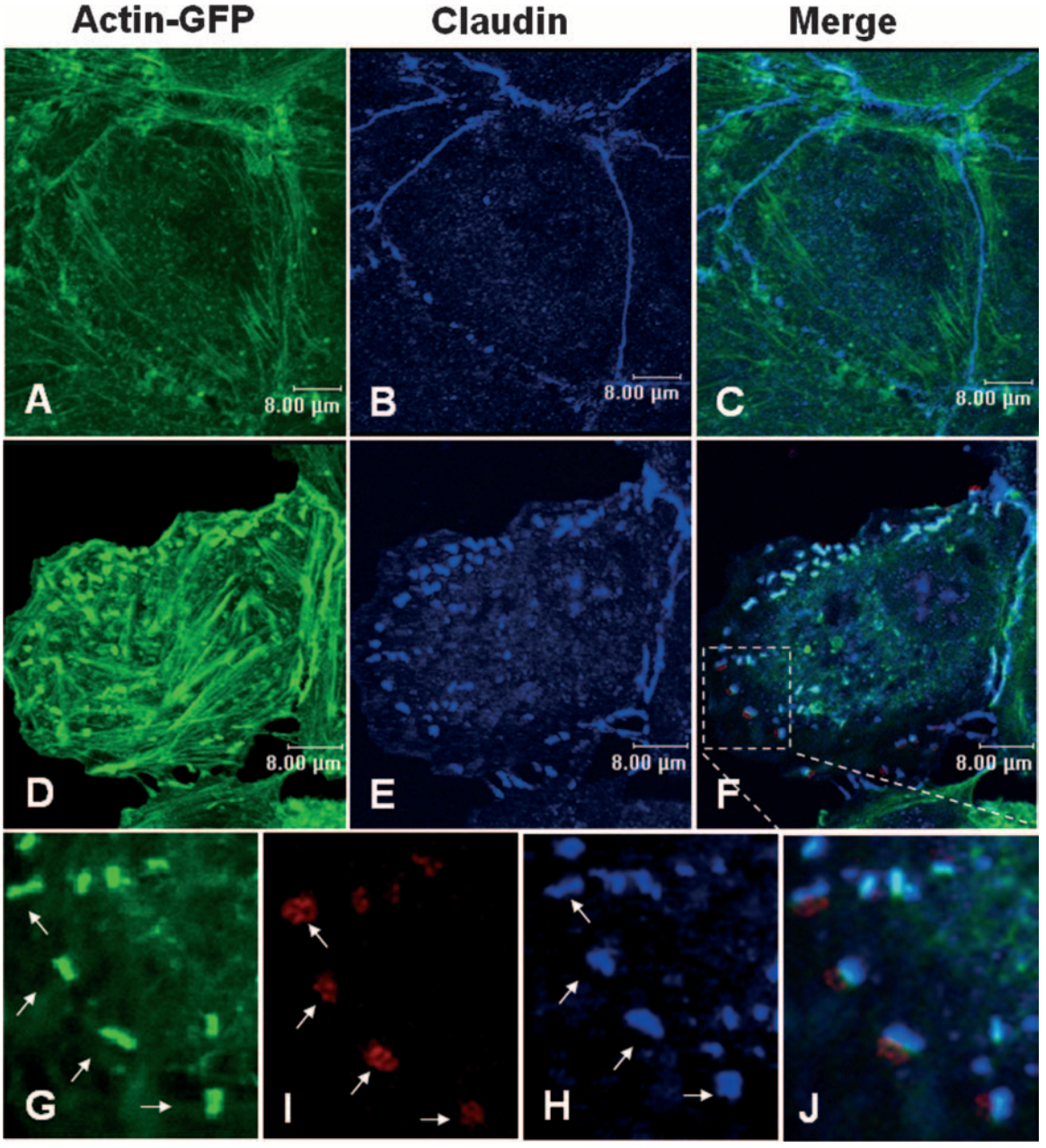

FIG. 8. REPEC induces claudin rearrangement and recruitment to pedestals in RK13 cells. (A to F) Rearrangement of claudin by REPEC (E22). Uninfected RK13 cells expressing actin-GFP (A) were fixed and stained with anti-claudin (B), and both images were merged (C). RK13 cells expressing actin-GFP (D) were infected with red fluorescent E22 (F) and fixed and stained with anti-claudin (E), and the images were merged (F). (G to J) REPEC recruits claudin to the pedestals. The magnification of panel F shows the specific localization of actin-GFP pedestals (G) beneath the attached red bacteria (H), which are enriched with claudin (I). The merged images show the colocalization of actin-GFP pedestals and claudin.

1 to 3 h), and the infected cells were fractionated into soluble (cytosol) and insoluble (membrane and cytoskeleton) fractions. Both fractions were treated with anti-EspF antibody, and the immunoprecipitates were subjected to Western blotting using anti-ZO-1, anti-ZO-2, anti-occludin, anti-claudin, anti-actin, and anti-EspF antibodies. In the soluble fraction, EspF did not interact with ZO-1 at 1, 1.5, and 2 h but EspF–ZO-1 interactions were detected at 2.5 and 3 h postinfection (Fig. 12A). In contrast, in the insoluble fraction, EspF strongly interacted with ZO-1 at 1 h postincubation and this interaction decreased with time until almost disappearing at 3 h postinfection (Fig. 12B). In the case of ZO-2, no interaction was detected with EspF in the soluble fraction at all times tested (Fig. 12A), but a weak interaction was observed in the insoluble fraction at 1 and 1.5 h postinfection; this weak reaction almost disappeared at subsequent time points (Fig. 12B). Furthermore, occludin and claudin were not coimmunoprecipitated by the anti-EspF antibody, suggesting that these two

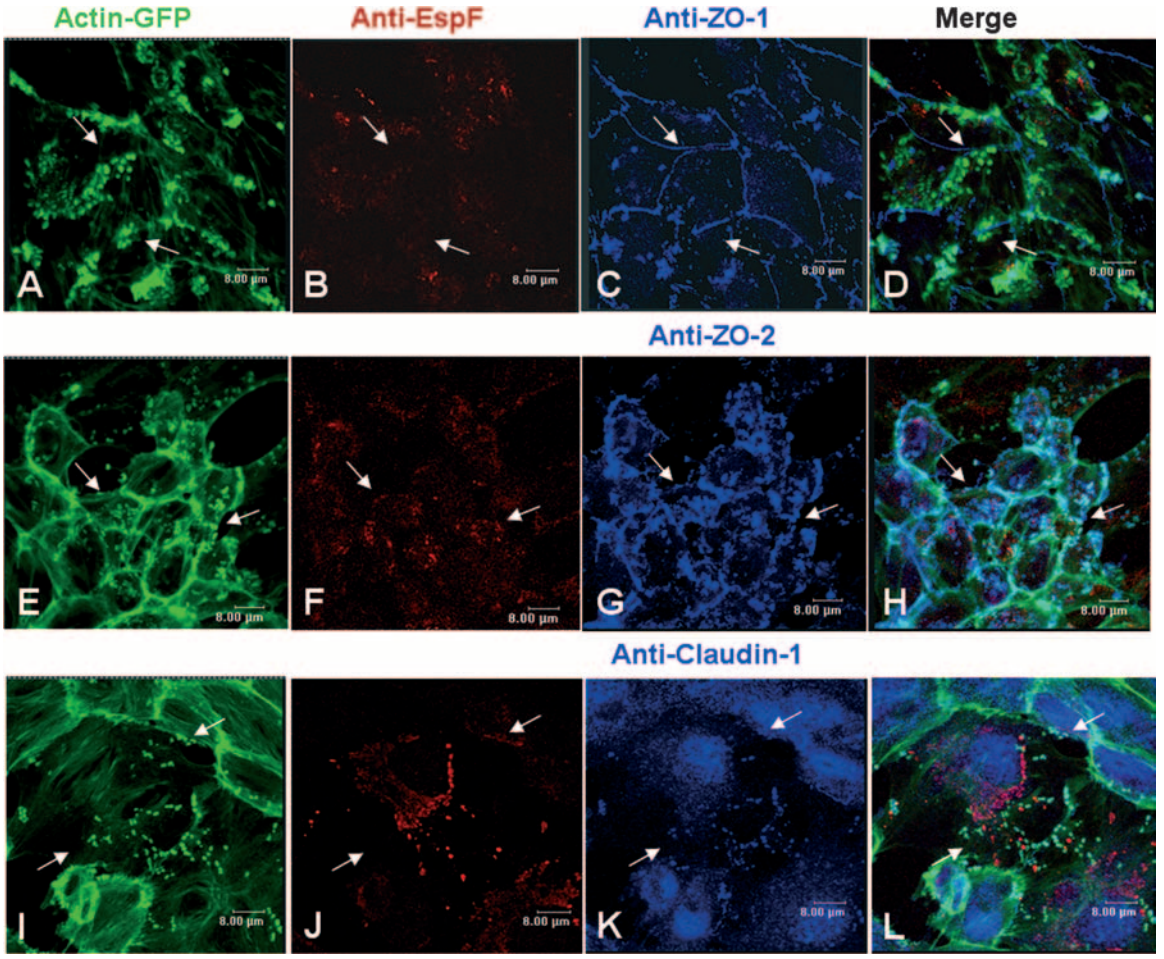

FIG. 9. EspF does not colocalize with ZO-1, ZO-2, or claudin into the pedestals, but it does so in nearby sites. RK13 cells expressing actin-GFP were infected with wild-type E22 for 3 h. Infected cells expressing actin-GFP (A, E, and I) were fixed and immunostaining by using anti-EspF (B, F, and J) and with anti ZO-1 (C), anti-ZO-2 (G), or anti-claudin 1 (K). Panel D is a merged image from panels A, B, and C; panel H is a merged image from panels E, F, and G; and panel L is a merged image from panels I, J, and K.

proteins do not interact directly (data not shown). Interestingly, in the soluble fraction, EspF had a strong interaction with actin at all time points tested (Fig. 12A), whereas only a slight interaction was detected in the insoluble fraction, mainly at 1 h postinfection, and it decreased until it disappeared 2 h after infection (Fig. 12B). Finally, anti-EspF immunoprecipitated EspF from both the soluble and the insoluble fractions of E22-infected RK13 cells (Fig. 12A and B). However, the 13-kDa protein species recognized by anti-EspF is not present in the immunoprecipitates from the insoluble fraction. As previously reported, two EspF species were detected in culture supernatants from E22-infected cells: the 23- and 13-kDa proteins. It is not yet clear why EspF appears on PAGE gels as multiple bands, but it seems that the low-molecular-weight EspF correlates to intracellular EspF following mitochondrial targeting signal cleavage upon mitochondrial import (33). These two proteins were not immunoprecipitated in uninfected cells, but both were detected in lysates from infected cells (data not shown). These latter results indicate that the 13-kDa protein is present only in the soluble fraction.

All of these data suggest that EspF does not interact directly with the transmembrane proteins occludin and claudin but does interact with the scaffold proteins ZO-1 and ZO-2 in the first hours of infection. This latter interaction may be related to the strong actin interaction observed at all the infection times tested, and this may lead to actin depolymerization in the TJ zones.

DISCUSSION

EspF is considered a multifunctional protein injected into host cells by A/E pathogens, but the mechanism of action of this effector is not understood completely. Here we show that EspF may act as a nucleation-promoting factor that participates in the regulation of actin polymerization by binding to actin directly or by binding indirectly through its interaction with profilin. EspF is able to bind ZO-1 and ZO-2 scaffold proteins, causing local actin depolymerization by sequestering actin and profilin and leading to disequilibrium of the polymerization-depolymerization cycles. EspF-induced actin depolymerization in the TJ could enable endocytosis of transmembrane junctional proteins (rearrangement of occludin and

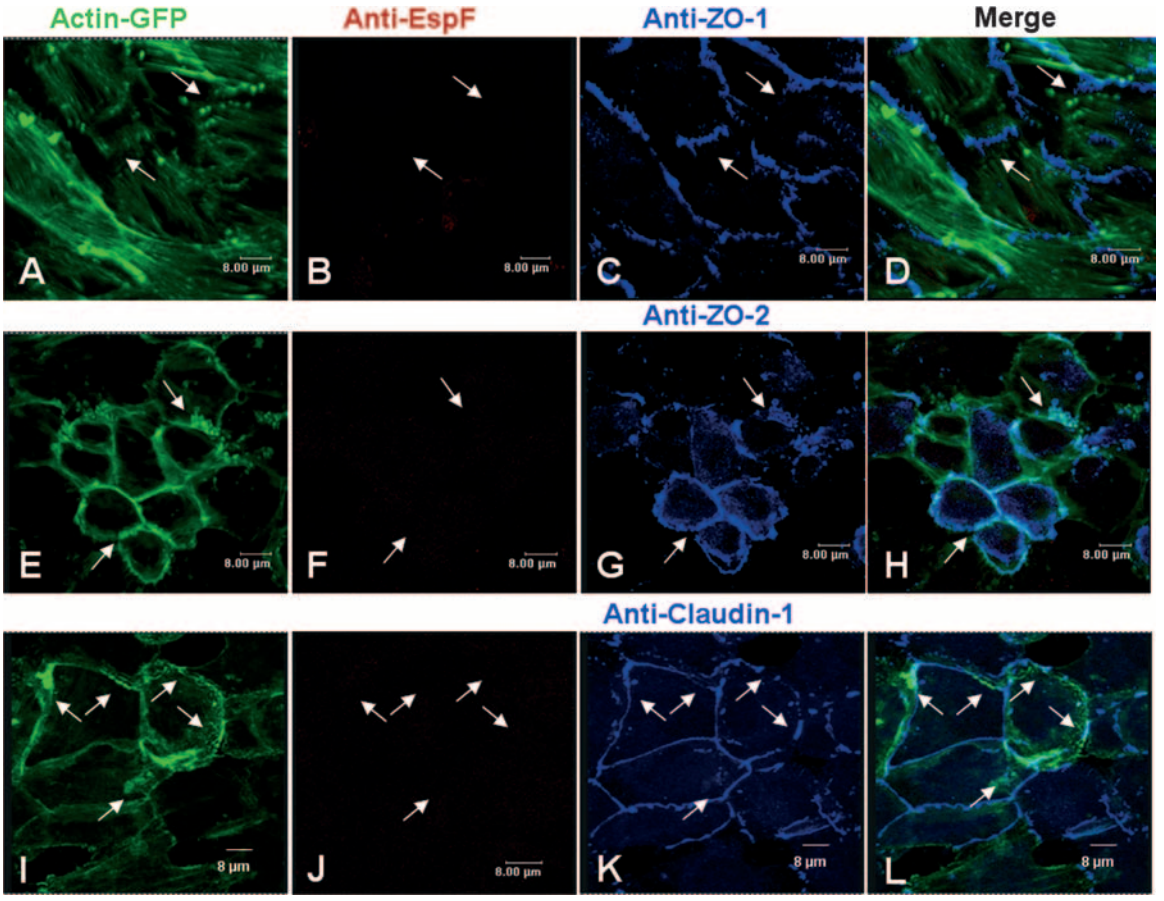

FIG. 10. An isogenic *espF* mutant does not cause redistribution of ZO-1, ZO-2, or claudin, and short pedestals are formed in the intercellular junctions. RK13 cells expressing actin-GFP were infected with the EspF mutant (E22 Δ*espF*) for 3 h. Infected cells expressing actin-GFP (A, E, and I) were fixed and immunostained by using anti-EspF (B, F, and J) and with anti ZO-1 (C), anti-ZO-2 (G), or anti-claudin-1 (K). Panel D is a merged image from panels A, B, and C; panel H is a merged image from panels E, F, and G; and panel L is a merged image from panels I, J, and K.

claudin). Thus, EspF favors recruitment of junctional proteins into the pedestals by sequestering actin, leading to maturation of actin pedestals and paracellular permeability disruption.

All the A/E pathogens containing the LEE pathogenicity island induce actin-rich pedestals and also TJ disruption (17), events which appear to be related. EspF is clearly associated with TJ disruption, but it has not been previously associated with pedestal formation (28). However, EspF contains motifs that may be related to these two aforementioned activities.

The PDZ domain binding motifs present in EspF (Fig. 1) may be important in the disruption of the TJ, since these motifs might be interacting with PDZ domains present in the membrane-associated guanylate kinase (MAGUK) family, which is characterized by the presence of several protein-protein interaction domains and whose members function as scaffolding factors that recruit signaling molecules to cell junctions and synaptic termini, including the ZO-1, ZO-2, and ZO-3 junctional proteins. Structural and molecular studies have shown that PDZ domains are pivotal features of scaffolding proteins and localize MAGUKs and their interaction partners to specialized membrane domains of neuronal and epithelial cells (10, 11). The domain architecture of the MAGUKs enables interaction with receptors, the actin cytoskeleton, and ion channels but also allows the tethering together of different MAGUK subfamily proteins (50), which may contain up to six PDZ domains (44).

EspF sequences from REPEC, EPEC, EHEC, and *C. rodentium* contain conserved repeated motifs that are located in the same position in their sequences, although the number of repeats can vary. These repeated sequences, proline-rich motifs and PDZ domain binding motifs, may be related to actin rearrangement and TJ disruption. These motifs in EspF proteins from different A/E pathogens may play a relevant role, since in all these A/E pathogens the EspF proteins have similar functions and are interchangeable (48). Here we showed that all EspFs share the proline-rich motif with WASP-related proteins, such as WASP, N-WASP, WAVE, and WIP, as well as Enah. The WASP family, WIP family, and Ena/VASP family share a related function as actin regulatory proteins in which their proline-rich motifs play a key role. WASP and N-WASP contain proline-rich sequences that can bind to SH3 domains and profilin. Profilin is a small protein that binds to an actin monomer and then supplies it to the barbed end (fast-growing end) of an actin filament (35). WIP, CR16, and WICH/WIRE contain between three and six potential profilin-binding sites named ABM-2 (*a*ctin-*b*ased *m*otility homology-*2*, which in-

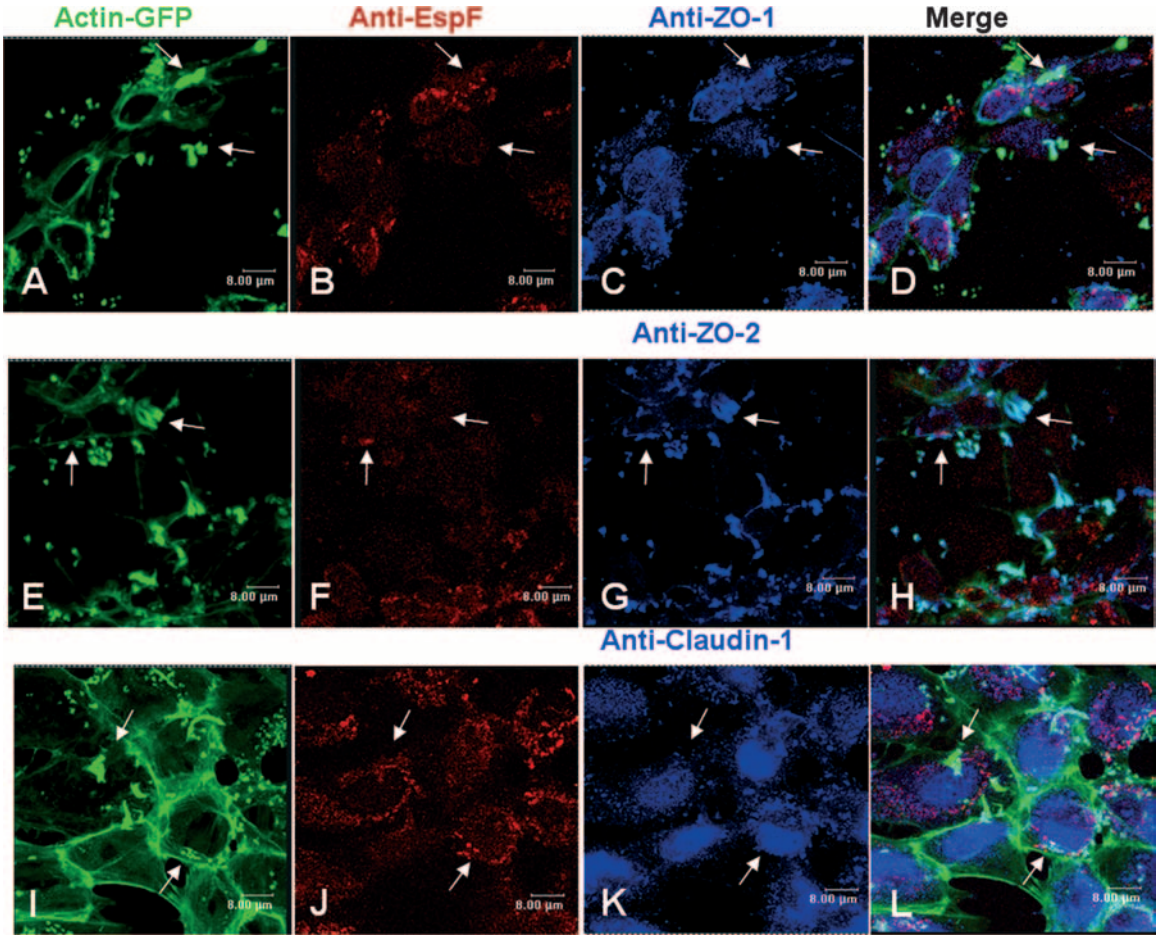

FIG. 11. EspF-overexpressing E22 causes enrichment of ZO-1, ZO-2, and claudin into the pedestals and increases in pedestal lengths. RK13 cells expressing actin-GFP were infected with wild-type E22 transformed with p*espF* for 3 h. Infected cells expressing actin-GFP (A, E, and I) were fixed and immunostained by using anti-EspF (B, F, and J) and with anti ZO-1 (C), anti-ZO-2 (G), or anti-claudin-1 (K). Panel D is a merged image from panels A, B, and C; panel H is a merged image from panels E, F, and G; and panel L is a merged image from panels I, J, and K.

cludes the sequence XPPPPP, where X is A, S, L, or G). In addition, profilin binds to both G- and F-actin (3). Our alignment and phylogenetic analysis of these proteins and EspF revealed that EspF is more closely related to WIP than to the WASP family and that EspF and these actin regulatory proteins share binding motifs, including APPPPP sequences, with profilin, actin, and Arp2/3, which are important proteins in the dynamics of actin polymerization. Interestingly, EspF was able to bind profilin, actin, WASP, and Arp2/3.

During REPEC infection, EspF interacts with WASP and Arp2/3 before 2 h postinfection, suggesting that these three proteins interact at the beginning of the infection and before the pedestal is formed; we believe that EspF is interacting directly with both proteins or mainly with WASP (and thereby indirectly to Arp2/3), but no experiments were performed to confirm this. Interestingly, EspF also interacts with ZO-1 and ZO-2 junctional proteins at the same times (before 2 h postinfection) in the insoluble fraction of infected cells, suggesting that all of these proteins are interacting in the polymerization-depolymerization cycles at the TJ (46). This idea is supported by the fact that EspF also contains PDZ domain binding motifs at exactly the same positions in the EspF orthologs (Fig. 1). PDZ domains are structurally conserved modules of 80 to 90 amino acids present in intracellular proteins. Their name originates from the three proteins where they were first identified (named PSD-95/Discs-large/ZO-1). The ability of PDZ domains to interact with proteins is well documented. They recognize motifs of 3 to 7 amino acids, termed PDZ binding motifs, that are generally present at the C-terminal ends of membrane proteins (51). With respect to the growing number of components constituting the multimolecular TJ complex, there is a group of proteins termed the TJ plaque proteins, many of which express PDZ domains, that serve as links between the integral TJ proteins and the actin cytoskeleton and as adapters for the recruitment of cytosolic molecules implicated in cell signaling (40). Unlike the interaction of EspF with N-WASP, Arp2/3, and ZO proteins, EspF interacts with profilin and actin throughout the course of REPEC infection (from 1 to 3 h). It this case, we were able to show that EspF interacts with both proteins, as the immunoprecipitation experiments showed that the anti-EspF antibody coimmunoprecipitated a large amount of actin in the soluble fraction (G-actin) and it also coimmunoprecipitated the actin that was binding to profilin. EspF also has homology with RickA, a

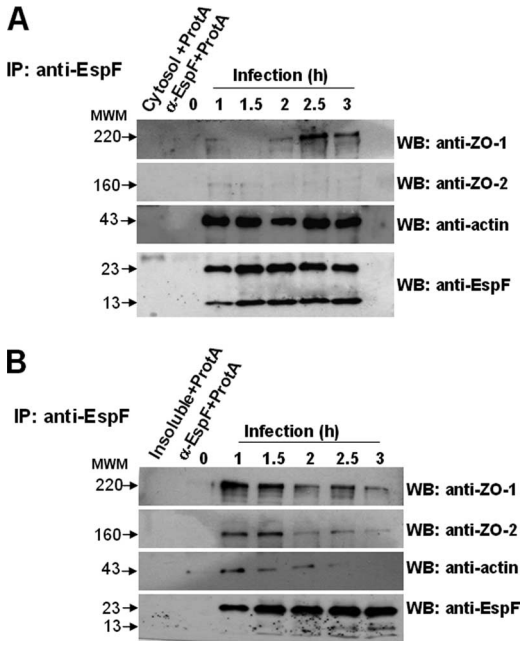

FIG. 12. EspF interacts with ZO-1, ZO-2, and actin in RK13 cells infected with E22. RK13 cells were infected with wild-type E22 for the indicated times. Infected cells were lysed by three cycles of freezing and thawing and passage through a needle. Lysed cells were centrifuged to obtain the soluble fraction. The pellet was washed in RIPA-0.1% SDS for 30 min, and then this fraction was recentrifuged to obtain the insoluble fraction (membrane proteins). Soluble (A) and insoluble (B) fractions were subjected to immunoprecipitation by using anti-EspF antibodies. Immunoprecipitates were separated by SDS-PAGE and transferred to nitrocellulose membrane to be probed with anti-ZO-1, anti-ZO-2, or anti-actin antibodies. Soluble or insoluble fractions plus protein-A agarose (Cytosol+ProtA) and anti-EspF antibody plus protein A-agarose (α-EspF+ProtA), as well as infection at time zero, were used as negative controls. IP, immunoprecipitation; WB, Western blotting; MWM, molecular weight marker.

Rickettsia WASP-like protein that activates the Arp2/3 complex and mediates actin-based motility.

Unusual WIP behavior in actin pedestals formed by EPEC and EHEC has been reported previously (22). Furthermore, WIP also inhibits actin depolymerization rates in a concentration-dependent manner; thus, members of the WIP family may increase cellular F-actin content by virtue of their ability to stabilize F-actin (18, 25). Additionally, WIP increases the efficiency of cortactin-mediated activation of the Arp2/3 complex in vitro and stimulates membrane protrusion in a manner dependent on an intact cortactin SH3 domain, which is responsible for binding the proline-rich region of WIP. Since TJs are intimately related to the perijunctional cytoskeleton, actin and/or profilin sequestration must cause actin depolymerization-induced TJ disruption (46). It has been shown that actin depolymerization disrupts TJs via caveola-mediated endocytosis of TJ proteins, such as occludin (41). Interestingly, here we show that actin depolymerization causes structural and functional TJ disruption by a pathophysiological process induced by EspF-producing bacteria, unlike what was found in studies using pharmacological actin disruptors. This hypothesis is supported by the fact that EspF-producing REPEC, but not the *espF* isogenic mutant, caused a redistribution of TJ proteins from the intercellular junction and a drop in TER values. These findings also indicate the key role of TJ proteins in the formation of pedestals due to the recruitment of these proteins into the pedestals in the cells by the wild-type strain or in the intracellular junctions by the isogenic mutant; these results also support the recent finding of ZO-1 recruitment into pedestals by a human EPEC strain (15). Moreover, the EspF mutant is unable to form mature pedestals and those that did form were very short in comparison with those induced by the wild-type strain and were even bigger when EspF was overexpressed by using E22 transformed with p*espF*, even though the number of pedestals appeared to be similar.

TJ protein endocytosis due to actin depolymerization, which is caused by actin and profilin sequestration by EspF, is also supported by recent findings on TJ disruption and pedestal formation. For instance, internalized occludin colocalizes with caveolin-1 and dynamin II, which is blocked by dominant negative dynamin II (K44A) and inhibition of caveola-mediated endocytosis by cholesterol extraction prevented both latrunculin A-induced TER loss and occludin internalization (41). Conversely, for EPEC infections, other authors have found that dynamin is required for F-actin assembly and pedestal formation by EPEC E2348/69 (47) and that EPEC E2348/69 Tir translocation and pedestal formation require membrane cholesterol (1). Recently, Alto et al. (2) also reported that that the type III effector EspF coordinates membrane remodeling and F-actin polymerization during EPEC pathogenesis, since EspF activated both SNX9 and N-WASP in a coordinated spatiotemporal pattern at clathrin-coated pits, again indicating a relationship between endocytosis and actin polymerization. However, even though EspF may actually represent a pathogenic strategy to mimic a natural host SNX9/N-WASP signaling complex (2), our data support the hypothesis that membrane trafficking is required for epithelial TJ maintenance and the formation of the apical/basolateral poles (49), since EspF promotes the internalization of TJ proteins in vivo (14), potentially through a membrane-trafficking phenotype. Moreover, SNX9, with an accessory role in the endocytic processes in that it binds clathrin, was initially identified as a host cell EspF binding partner protein; EspF specifically interacts with membrane-bound SNX9 by using the SH3 domain and no coimmunoprecipitation was detected with the cytosolic fraction of SNX9 (23).

ACKNOWLEDGMENTS

We thank Ian Henderson for invaluable critical review of the manuscript and Lourdes Ruiz, Hector Salazar-Gonzalez, Lucia Chavez, and Claudia Marquez for their technical help.

This work was supported by grants from Consejo Nacional de Ciencia y Tecnología de México (CONACYT, 60714 and C02-44660) to F.N.-G.

REFERENCES

1. **Allen-Vercoe, E., B. Waddell, S. Livingstone, J. Deans, and R. DeVinney.** 2006. Enteropathogenic *Escherichia coli* Tir translocation and pedestal formation requires membrane cholesterol in the absence of bundle-forming pili. Cell. Microbiol. **8:**613–624.
2. **Alto, N. M., A. W. Weflen, M. J. Rardin, D. Yarar, C. S. Lazar, R. Tonikian, A. Koller, S. S. Taylor, C. Boone, S. S. Sidhu, S. L. Schmid, G. A. Hecht, and J. E. Dixon.** 2007. The type III effector EspF coordinates membrane trafficking by the spatiotemporal activation of two eukaryotic signaling pathways. J. Cell Biol. **178:**1265–1278.
3. **Aspenstrom, P.** 2004. The mammalian verprolin homologue WIRE partici-

pates in receptor-mediated endocytosis and regulation of the actin filament system by distinct mechanisms. Exp. Cell Res. **298:**485–498.
4. **Ben-Ami, G., V. Ozeri, E. Hanski, F. Hofmann, K. Aktories, K. M. Hahn, G. M. Bokoch, and I. Rosenshine.** 1998. Agents that inhibit Rho, Rac, and Cdc42 do not block formation of actin pedestals in HeLa cells infected with enteropathogenic *Escherichia coli*. Infect. Immun. **66:**1755–1758.
5. **Campellone, K. G., A. Giese, D. J. Tipper, and J. M. Leong.** 2002. A tyrosine-phosphorylated 12-amino-acid sequence of enteropathogenic *Escherichia coli* Tir binds the host adaptor protein Nck and is required for Nck localization to actin pedestals. Mol. Microbiol. **43:**1227–1241.
6. **Campellone, K. G., and J. M. Leong.** 2005. Nck-independent actin assembly is mediated by two phosphorylated tyrosines within enteropathogenic *Escherichia coli* Tir. Mol. Microbiol. **56:**416–432.
7. **Campellone, K. G., S. Rankin, T. Pawson, M. W. Kirschner, D. J. Tipper, and J. M. Leong.** 2004. Clustering of Nck by a 12-residue Tir phosphopeptide is sufficient to trigger localized actin assembly. J. Cell Biol. **164:**407–416.
8. **Cossart, P., and P. J. Sansonetti.** 2004. Bacterial invasion: the paradigms of enteroinvasive pathogens. Science **304:**242–248.
9. **Datsenko, K. A., and B. L. Wanner.** 2000. One-step inactivation of chromosomal genes in *Escherichia coli* K-12 using PCR products. Proc. Natl. Acad. Sci. USA **97:**6640–6645.
10. **Funke, L., S. Dakoji, and D. S. Bredt.** 2005. Membrane-associated guanylate kinases regulate adhesion and plasticity at cell junctions. Annu. Rev. Biochem. **74:**219–245.
11. **Gonzalez-Mariscal, L., A. Betanzos, and A. Avila-Flores.** 2000. MAGUK proteins: structure and role in the tight junction. Semin. Cell Dev. Biol. **11:**315–324.
12. **Goosney, D. L., R. DeVinney, and B. B. Finlay.** 2001. Recruitment of cytoskeletal and signaling proteins to enteropathogenic and enterohemorrhagic *Escherichia coli* pedestals. Infect. Immun. **69:**3315–3322.
13. **Gruenheid, S., and B. B. Finlay.** 2003. Microbial pathogenesis and cytoskeletal function. Nature **422:**775–781.
14. **Guttman, J. A., Y. Li, M. E. Wickham, W. Deng, A. W. Vogl, and B. B. Finlay.** 2006. Attaching and effacing pathogen-induced tight junction disruption *in vivo*. Cell. Microbiol. **8:**634–645.
15. **Hanajima-Ozawa, M., T. Matsuzawa, A. Fukui, S. Kamitani, H. Ohnishi, A. Abe, Y. Horiguchi, and M. Miyake.** 2007. Enteropathogenic *Escherichia coli*, *Shigella flexneri*, and *Listeria monocytogenes* recruit a junctional protein, zonula occludens-1, to actin tails and pedestals. Infect. Immun. **75:**565–573.
16. **Kalman, D., O. D. Weiner, D. L. Goosney, J. W. Sedat, B. B. Finlay, A. Abo, and J. M. Bishop.** 1999. Enteropathogenic *E. coli* acts through WASP and Arp2/3 complex to form actin pedestals. Nat. Cell Biol. **1:**389–391.
17. **Kaper, J. B., J. P. Nataro, and H. L. Mobley.** 2004. Pathogenic *Escherichia coli*. Nat. Rev. Microbiol. **2:**123–140.
18. **Kato, M., H. Miki, S. Kurita, T. Endo, H. Nakagawa, S. Miyamoto, and T. Takenawa.** 2002. WICH, a novel verprolin homology domain-containing protein that functions cooperatively with N-WASP in actin-microspike formation. Biochem. Biophys. Res. Commun. **291:**41–47.
19. **Kenny, B., R. DeVinney, M. Stein, D. J. Reinscheid, E. A. Frey, and B. B. Finlay.** 1997. Enteropathogenic *E. coli* (EPEC) transfers its receptor for intimate adherence into mammalian cells. Cell **91:**511–520.
20. **Knutton, S., T. Baldwin, P. H. Williams, and A. S. McNeish.** 1989. Actin accumulation at sites of bacterial adhesion to tissue culture cells: basis of a new diagnostic test for enteropathogenic and enterohemorrhagic *Escherichia coli*. Infect. Immun. **57:**1290–1298.
21. **Laemmli, U. K.** 1970. Cleavage of structural proteins during the assembly of the head of bacteriophage T4. Nature **227:**680–685.
22. **Lommel, S., S. Benesch, M. Rohde, J. Wehland, and K. Rottner.** 2004. Enterohaemorrhagic and enteropathogenic *Escherichia coli* use different mechanisms for actin pedestal formation that converge on N-WASP. Cell. Microbiol. **6:**243–254.
23. **Marches, O., M. Batchelor, R. K. Shaw, A. Patel, N. Cummings, T. Nagai, C. Sasakawa, S. R. Carlsson, R. Lundmark, C. Cougoule, E. Caron, S. Knutton, I. Connerton, and G. Frankel.** 2006. EspF of enteropathogenic *Escherichia coli* binds sorting nexin 9. J. Bacteriol. **188:**3110–3115.
24. **Marches, O., J. P. Nougayrede, S. Boullier, J. Mainil, G. Charlier, I. Raymond, P. Pohl, M. Boury, J. De Rycke, A. Milon, and E. Oswald.** 2000. Role of Tir and intimin in the virulence of rabbit enteropathogenic *Escherichia coli* serotype O103:H2. Infect. Immun. **68:**2171–2182.
25. **Martinez-Quiles, N., R. Rohatgi, I. M. Anton, M. Medina, S. P. Saville, H. Miki, H. Yamaguchi, T. Takenawa, J. H. Hartwig, R. S. Geha, and N. Ramesh.** 2001. WIP regulates N-WASP-mediated actin polymerization and filopodium formation. Nat. Cell Biol. **3:**484–491.
26. **McDaniel, T. K., K. G. Jarvis, M. S. Donnenberg, and J. B. Kaper.** 1995. A genetic locus of enterocyte effacement conserved among diverse enterobacterial pathogens. Proc. Natl. Acad. Sci. USA **92:**1664–1668.
27. **McNamara, B. P., and M. S. Donnenberg.** 1998. A novel proline-rich protein, EspF, is secreted from enteropathogenic *Escherichia coli* via the type III export pathway. FEMS Microbiol. Lett. **166:**71–78.
28. **McNamara, B. P., A. Koutsouris, C. B. O'Connell, J. P. Nougayrede, M. S. Donnenberg, and G. Hecht.** 2001. Translocated EspF protein from enteropathogenic *Escherichia coli* disrupts host intestinal barrier function. J. Clin. Investig. **107:**621–629.
29. **Moon, H. W., S. C. Whipp, R. A. Argenzio, M. M. Levine, and R. A. Giannella.** 1983. Attaching and effacing activities of rabbit and human enteropathogenic *Escherichia coli* in pig and rabbit intestines. Infect. Immun. **41:**1340–1351.
30. **Moreau, V., F. Frischknecht, I. Reckmann, R. Vincentelli, G. Rabut, D. Stewart, and M. Way.** 2000. A complex of N-WASP and WIP integrates signalling cascades that lead to actin polymerization. Nat. Cell Biol. **2:**441–448.
31. **Mullins, R. D.** 2000. How WASP-family proteins and the Arp2/3 complex convert intracellular signals into cytoskeletal structures. Curr. Opin. Cell Biol. **12:**91–96.
32. **Muza-Moons, M. M., E. E. Schneeberger, and G. A. Hecht.** 2004. Enteropathogenic *Escherichia coli* infection leads to appearance of aberrant tight junctions strands in the lateral membrane of intestinal epithelial cells. Cell. Microbiol. **6:**783–793.
33. **Nougayrede, J. P., and M. S. Donnenberg.** 2004. Enteropathogenic *Escherichia coli* EspF is targeted to mitochondria and is required to initiate the mitochondrial death pathway. Cell. Microbiol. **6:**1097–1111.
34. **Nougayrede, J. P., G. H. Foster, and M. S. Donnenberg.** 2007. Enteropathogenic *Escherichia coli* effector EspF interacts with host protein Abcf2. Cell. Microbiol. **9:**680–693.
35. **Pantaloni, D., and M. F. Carlier.** 1993. How profilin promotes actin filament assembly in the presence of thymosin beta 4. Cell **75:**1007–1014.
36. **Phillips, N., R. D. Hayward, and V. Koronakis.** 2004. Phosphorylation of the enteropathogenic *E. coli* receptor by the Src-family kinase c-Fyn triggers actin pedestal formation. Nat. Cell Biol. **6:**618–625.
37. **Philpott, D. J., D. M. McKay, P. M. Sherman, and M. H. Perdue.** 1996. Infection of T84 cells with enteropathogenic *Escherichia coli* alters barrier and transport functions. Am. J. Physiol. **270:**G634–G645.
38. **Rohatgi, R., P. Nollau, H. Y. Ho, M. W. Kirschner, and B. J. Mayer.** 2001. Nck and phosphatidylinositol 4,5-bisphosphate synergistically activate actin polymerization through the N-WASP-Arp2/3 pathway. J. Biol. Chem. **276:**26448–26452.
39. **Sanger, J. M., R. Chang, F. Ashton, J. B. Kaper, and J. W. Sanger.** 1996. Novel form of actin-based motility transports bacteria on the surfaces of infected cells. Cell Motil. Cytoskeleton **34:**279–287.
40. **Schneeberger, E. E., and R. D. Lynch.** 2004. The tight junction: a multifunctional complex. Am. J. Physiol. Cell Physiol. **286:**C1213–C1228.
41. **Shen, L., and J. R. Turner.** 2005. Actin depolymerization disrupts tight junctions via caveolae-mediated endocytosis. Mol. Biol. Cell **16:**3919–3936.
42. **Simonovic, I., J. Rosenberg, A. Koutsouris, and G. Hecht.** 2000. Enteropathogenic *Escherichia coli* dephosphorylates and dissociates occludin from intestinal epithelial tight junctions. Cell. Microbiol. **2:**305–315.
43. **Stebbins, C. E., and J. E. Galan.** 2001. Structural mimicry in bacterial virulence. Nature **412:**701–705.
44. **Te Velthuis, A. J., J. F. Admiraal, and C. P. Bagowski.** 2007. Molecular evolution of the MAGUK family in metazoan genomes. BMC Evol. Biol. **7:**129.
45. **Towbin, H., T. Staehelin, and J. Gordon.** 1979. Electrophoretic transfer of proteins from polyacrylamide gels to nitrocellulose sheets: procedure and some applications. Proc. Natl. Acad. Sci. USA **76:**4350–4354.
46. **Turner, J. R.** 2006. Molecular basis of epithelial barrier regulation: from basic mechanisms to clinical application. Am. J. Pathol. **169:**1901–1909.
47. **Unsworth, K. E., P. Mazurkiewicz, F. Senf, M. Zettl, M. McNiven, M. Way, and D. W. Holden.** 2007. Dynamin is required for F-actin assembly and pedestal formation by enteropathogenic *Escherichia coli* (EPEC). Cell. Microbiol. **9:**438–449.
48. **Viswanathan, V. K., A. Koutsouris, S. Lukic, M. Pilkinton, I. Simonovic, M. Simonovic, and G. Hecht.** 2004. Comparative analysis of EspF from enteropathogenic and enterohemorrhagic *Escherichia coli* in alteration of epithelial barrier function. Infect. Immun. **72:**3218–3227.
49. **Wells, C. D., J. P. Fawcett, A. Traweger, Y. Yamanaka, M. Goudreault, K. Elder, S. Kulkarni, G. Gish, C. Virag, C. Lim, K. Colwill, A. Starostine, P. Metalnikov, and T. Pawson.** 2006. A Rich1/Amot complex regulates the Cdc42 GTPase and apical-polarity proteins in epithelial cells. Cell **125:**535–548.
50. **Zhang, Y., S. Yeh, B. A. Appleton, H. A. Held, P. J. Kausalya, D. C. Phua, W. L. Wong, L. A. Lasky, C. Wiesmann, W. Hunziker, and S. S. Sidhu.** 2006. Convergent and divergent ligand specificity among PDZ domains of the LAP and zonula occludens (ZO) families. J. Biol. Chem. **281:**22299–22311.
51. **Zimmermann, P.** 2006. The prevalence and significance of PDZ domain-phosphoinositide interactions. Biochim. Biophys. Acta **1761:**947–956.

Editor: V. J. DiRita